Three-Dimensional Solution Structure of ω-Conotoxin TxVII, an L-Type Calcium Channel Blocker[†,‡]

Kuniko Kobayashi, Toru Sasaki, Kazuki Sato,[§] and Toshiyuki Kohno*

Mitsubishi Kasei Institute of Life Sciences, Minamiooya, Machida, Tokyo 194-8511, Japan

Received June 30, 2000; Revised Manuscript Received September 27, 2000

ABSTRACT: We determined the three-dimensional structure of ω-conotoxin TxVII, a 26-residue peptide that is an L-type calcium channel blocker, by ^{1}H NMR in aqueous solution. Twenty converged structures of this peptide were obtained on the basis of 411 distance constraints obtained from nuclear Overhauser effect connectivities, 20 torsion angle constraints, and 21 constraints associated with hydrogen bonds and disulfide bonds. The root-mean-square deviations about the averaged coordinates of the backbone atoms (N, C_α, C, and O) and all heavy atoms were 0.50 ± 0.09 Å and 0.99 ± 0.13 Å, respectively. The structure of ω-conotoxin TxVII is composed of a triple-stranded antiparallel β-sheet and four turns. The three disulfide bonds in ω-conotoxin TxVII form the classical cystine knot motif of toxic or inhibitory polypeptides. The overall folding of ω-conotoxin TxVII is similar to those of the N-type calcium channel blockers, ω-conotoxin GVIA and MVIIA, despite the low amino acid sequence homology among them. ω-Conotoxin TxVII exposes many hydrophobic residues to a certain surface area. In contrast, ω-conotoxin GVIA and MVIIA expose basic residues in the same way as ω-conotoxin TxVII. The channel binding site of ω-conotoxin TxVII is different from those of ω-conotoxin GVIA and MVIIA, although the overall folding of these three peptides is similar. The gathered hydrophobic residues of ω-conotoxin TxVII probably interact with the hydrophobic cluster of the α_1 subunit of the L-type calcium channel, which consists of 13 residues located in segments 5 and 6 in domain III and in segment 6 in domain IV.

Voltage-gated calcium channels are classified into several subtypes, according to their electrophysiological and pharmacological features (*1*−*3*). Various ω-conotoxins from the venoms of marine snails block diverse ion channels and neurotransmitter receptors. Due to their various blocking activities, these peptide toxins are used as reagents to pharmacologically probe the functions of channels and receptors. The ω-conotoxin GVIA (ω-CTX GVIA[1]) from *Conus geographus* and the ω-conotoxin MVIIA (ω-CTX MVIIA) from *Conus magus* are well-known as examples of reagents that specifically block N-type voltage-sensitive calcium channels (*4*). ω-CTX GVIA and MVIIA are composed of 27 and 25 amino acid residues, respectively, including six Cys residues that form three disulfide bonds. In our previous study, we showed that the replacement of Tyr13 with Ala resulted in about 1000 times reduction in the binding affinity and that Tyr13 of ω-CTX GVIA and MVIIA is essential for the binding to the channel (*5, 6*). We also showed that the replacement of Lys2 with Ala resulted in about 40 times reduction in the binding affinity and that Lys2 is also important for the binding (*7*). The three-dimensional structures of ω-CTX GVIA (*8*−*12*) and MVIIA (*13, 14*) were determined by NMR spectroscopy. Functional and structural analyses revealed that both ω-CTX GVIA and MVIIA retain a similar conformation to place Lys2 and Tyr13 in the appropriate position to bind to N-type calcium channels.

L-Type calcium channels are pharmacologically defined by using the dihydropyridine (DHP) family as probes (*15, 16*). Calciseptine from snake venom (*17*) and ω-agatoxin IIIA from the spider venom (*18*) are the only known peptide toxins blocking L-type calcium channels, although they possess weak efficacy and low specificity. Recently, a novel ω-conotoxin, ω-conotoxin TxVII (ω-CTX TxVII), derived from the venom of the molluscivorous marine snail, *Conus textile*, was found to block the DHP-sensitive L-type calcium channels (*19*). ω-CTX TxVII consists of 26 amino acid residues with three disulfide bonds, similar to ω-CTX GVIA and MVIIA. ω-CTX TxVII has the 6-Cys/4-loop cysteine framework (*20*), $CX_nCX_nCCX_nCX_nC$, where C represents a

[†] This work was supported in part by a project grant from the Japan Health Science Foundation, Program for Promotion of Fundamental Studies in Health Sciences of Organization for Drug ADR Relief, R&D Promotion and Product Review of Japan.

[‡] Atomic coordinates for the 20 converged structures of ω-conotoxin TxVII have been deposited in the Protein Data Bank for release upon publication (accession code 1F3K).

* To whom correspondence should be addressed. Tel: +81-42-724-6285. Fax: +81-42-724-6296. E-mail: tkohno@libra.ls.m-kagaku.co.jp.

[§] Present address: Faculty of Human Environmental Science, Fukuoka Women's University, Kasumigaoka, Higashi-ku, Fukuoka 813-8529, Japan.

[1] Abbreviations: BTZ, benzothiazepine; CTX, conotoxin; DHP, dihydropyridine; DQF-COSY, double quantum-filtered correlation spectroscopy; DSS, 4,4-dimethyl-4-silapentane-1-sulfonic acid; MALDI-TOF-MS, matrix-assisted laser desorption/ionization time-of-flight mass spectrometry; NOE, nuclear Overhauser effect; NOESY, NOE spectroscopy; NMR, nuclear magnetic resonance; PAA, phenylalkylamine; PE-COSY, primitive exclusive correlation spectroscopy; PDB, protein data bank; RMS, root-mean-square; RMSD, root-mean-square deviation; RP-HPLC, reversed-phase high-performance liquid chromatography; TOCSY, total correlation spectroscopy; ω-CTX GVIA, ω-conotoxin GVIA; ω-CTX MVIIA, ω-conotoxin MVIIA; ω-CTX TxVII, ω-conotoxin TxVII. Standard abbreviations are used for amino acids.

10.1021/bi001506x CCC: $19.00
Published on Web 11/04/2000

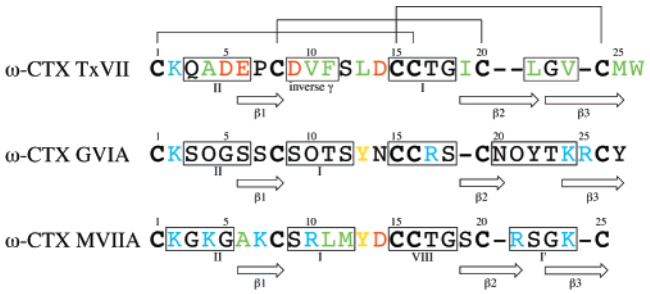

FIGURE 1: Comparative arrangements of amino acid sequences, based on the distribution of secondary structure elements and disulfide bonds in ω-CTX TxVII, GVIA, and MVIIA. The amino acid denoted O represents hydroxyproline, and the lines indicate disulfide bridges. Cys residues are shown in bold letters, and disulfide connectivities are also indicated. Blue, red, and green indicate basic, acidic, and hydrophobic residues, respectively. Each yellow residue in ω-conotoxin GVIA and MVIIA represents the residue essential for the activity. Six Cys residues are shown in bold letters and form three disulfide bonds. Note that Lys2 is conserved among these three conotoxins. Arrows and rectangles represent β-strands and turns, respectively.

cysteine residue and X represents any other residue. The framework is generally conserved in other toxic or inhibitory polypeptides, as in ω-CTX GVIA and MVIIA (Figure 1).

Although the backbone structure of ω-CTX TxVII is similar to those of ω-CTX GVIA and MVIIA, its calcium channel subtype specificity is quite different. Therefore, to elucidate the structural differences that determine the toxin selectivity for the L- and N-type calcium channels, ω-CTX TxVII is the most appropriate representative of the L-type calcium channel blockers. In this study, we determined for the first time the three-dimensional structure of the L-type calcium channel antagonist, ω-CTX TxVII, in aqueous solutions by using two-dimensional NMR with simulated annealing calculations. We evaluated the structure−activity relationships of ω-CTX TxVII on the basis of the structures of ω-CTX TxVII, GVIA, and MVIIA to elucidate the channel subtype recognition mechanism of these conotoxins.

MATERIALS AND METHODS

Peptide Synthesis. ω-CTX TxVII was chemically synthesized by the same strategy as described previously (*21*). The primary structure and the purity of ω-CTX TxVII were confirmed by analytical reversed-phase high-performance liquid chromatography (RP-HPLC), matrix-assisted laser desorption/ionization time-of-flight mass spectrometry (MALDI-TOF-MS) measurement, and amino acid analysis. The chemical and biological properties of the synthesized ω-CTX TxVII were confirmed by the mothod described (*21*).

NMR Spectroscopy. Samples for NMR experiments were 5 mM of ω-CTX TxVII dissolved in either 99.96% D_2O or 90% H_2O/10% D_2O (v/v) at pH 5.6 (uncorrected meter readings). NMR measurements were performed using standard pulse sequences and phase cycling with a Bruker AMX-500 or DRX-500 spectrometer. All two-dimensional NMR spectra were acquired in a phase-sensitive mode using time-proportional phase incrementation for quadrature detection in the t_1 dimension.

Spectra were processed by using UXNMR or XWIN NMR software. Phase-shifted sine-squared window functions were applied before Fourier transformation, with shifts of 60° or 90° in both dimensions. Final matrix sizes were usually 2048 × 2048 real points, except for PE-COSY (*22*). High-resolution DQF-COSY (*23*) and PE-COSY spectra were strip transformed to 1024 × 8192.

The following ^{1}H NMR spectra were recorded: DQF-COSY, NOESY (*24*, *25*) with mixing times of 100, 200, and 300 ms, TOCSY using a MLEV-17 pulse scheme (*26*) with isotropic mixing times of 65 ms, and PE-COSY. These spectra were recorded at 288, 298, and 310 K. The spectral width was 6250 Hz, and the data size used for acquisition was 512 (t_1) × 2048 (t_2), except for PE-COSY. High-resolution DQF-COSY and PE-COSY spectra were recorded to obtain the constraints for torsion angle and stereospecific assignments, and these data sizes for acquisition were 512 × 8192. Selective irradiation during the relaxation delay period was used to suppress the solvent resonance.

To identify the slow exchange of backbone amide protons, the sample lyophilized from an H_2O solution was redissolved in D_2O. NOESY spectra with a mixing time of 200 ms were measured after 20 min and 2 h, and subsequently every 1.5 h up to 76 h.

Chemical shifts were referenced to the methyl resonance of 4,4-dimethyl-4-silapentane-1-sulfonic acid (DSS) used as an internal standard. A complete set of the two-dimensional spectra was recorded at 288 K and pH 5.6.

Dihedral Angles and Stereospecific Assignments. The backbone NH-C_αH coupling constants were estimated by the DQF-COSY spectrum and were converted to the backbone torsion angle ϕ constraints according to the following rules: for $^3J_{NH-C\alpha H}$ less than 5.5 Hz, the ϕ angle was constrained in the range of $-65 \pm 25°$; for $^3J_{NH-C\alpha H}$ greater than 8.0 Hz, it was constrained in the range of $-120 \pm 40°$ (*27*, *28*). Backbone dihedral constraints were not applied for $^3J_{NH-C\alpha H}$ values between 5.5 and 8.0 Hz.

The range of the χ^1 side chain torsion angle constraints and the stereospecific assignment of the prochiral β-methylene protons were obtained by using the $^3J_{\alpha\beta}$ coupling constants combined with the intraresidue NH-C_βH NOEs (*29*). The $^3J_{\alpha\beta}$ coupling constants were determined from the PE-COSY spectrum in D_2O. For the t^2g^3, g^2g^3, and g^2t^3 conformations around the C_α-C_β bonds, the χ^1 side chain torsion angle was constrained in the ranges of $-60 \pm 40°$, $60 \pm 40°$, and $180 \pm 40°$ (*30*).

Distance Restraints and Structure Calculations. Quantitative determination of the cross-peak intensities was based on the counting of the contour levels. All NOE data were classified into strong, medium, weak, and very weak categories; each corresponds to upper bounds on interproton distances of 2.5, 3.5, 5.0, and 6.0 Å. Lower distance bounds were set to 1.8 Å for all categories. Appropriate pseudoatom corrections were applied to nonstereospecific-assigned protons (*31*). In addition, 0.5 Å was added to the upper limits for distance restraints involving methyl protons (*32*). Nine additional constraints were added to define the three disulfide bonds involved in ω-CTX TxVII. For each disulfide bond, there are three distance constraints, S(i)-S(j), S(i)-C_β(j), and S(j)-C_β(i), whose target values were set to 2.02 ± 0.02, 2.99 ± 0.50, and 2.99 ± 0.50 Å, respectively (*33*). After the initial calculation, 10 clearly defined distance constraints for five hydrogen bonds (24CO-5NH, 9CO-11NH, 2CO-16NH, 15CO-18NH, 20CO-22NH, and 6CO-24NH) were added as target values of 1.8−2.3 Å for NH(i)-O(j) and 2.8−3.3 Å for N(i)-O(j), respectively.

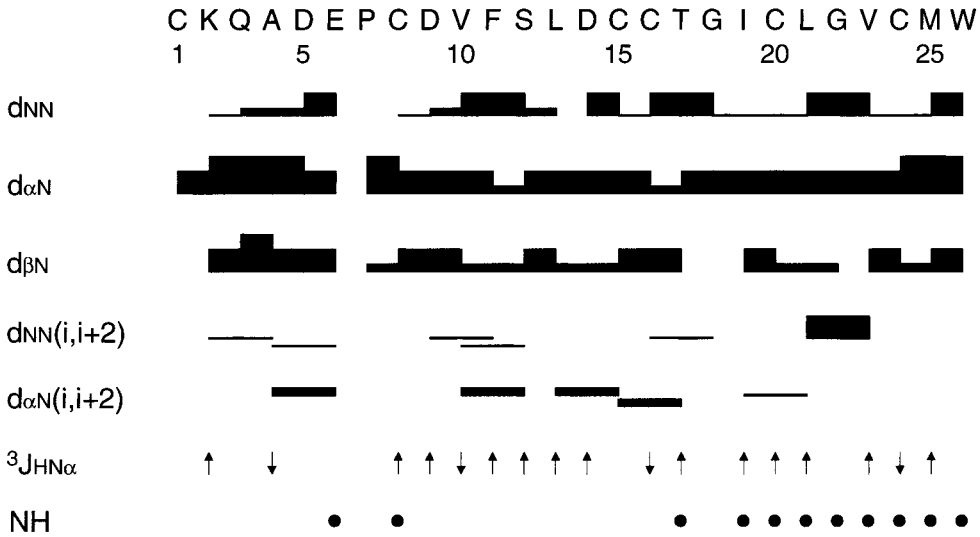

FIGURE 2: NMR data summary of ω-CTX TxVII. Sequential and medium range NOE connectivities, $^3J_{NH-C\alpha H}$ coupling constants, and slowly exchanging backbone NH protons are shown. Sequential and medium range NOEs, d_{NN}, $d_{\alpha N}$, $d_{\beta N}$, $d_{NN}(i, i+2)$, and $d_{\alpha N}(i, i+2)$, are indicated by bars between two residues. The NOEs are classified into strong, medium, weak, and very weak, according to the height of the filled bars. The values of the $^3J_{NH-C\alpha H}$ coupling constants are indicated by ↑ (> 8 Hz) and ↓ (<5.5 Hz). Filled circles indicate backbone amide protons that were still observed in the NOESY spectra after 76 h in D_2O.

Three-dimensional structures were calculated on the basis of the experimentally derived distance and torsion angle constraints, using a dynamically simulated annealing protocol. The annealing started from a template structure with randomized ϕ and ψ dihedral angles in X-PLOR version 3.1 (*34*).

Evaluation of the Structure. The final structures with the lowest energy and small Lennard-Jones van der Waals energy were chosen. The convergence of the calculated structures was evaluated in terms of the structural parameters. There are RMS deviations from the experimental distance and dihedral constraints and the values of the energetic statistics (F_{NOE}, F_{tor}, F_{repel}, and E_{L-J}), and RMS deviations from the idealized geometry. The distributions of the backbone dihedral angles of the final converged structures were evaluated by the representation of the Ramachandran dihedral pattern, indicating the deviations from the allowed (ϕ, ψ) angle limits (*35*). The degrees of angular variation among the converged structures were further assessed by using an angular order parameter (*8*, *36*).

RESULTS

Assignments of ^{1}H Resonances, Dihedral Angles, and Stereospecific Assignments. All ^{1}H resonances in the spectrum were assigned in a straightforward manner by applying the sequential assignment method, pioneered by Wüthrich (*37*), to a combination of COSY, TOCSY, and NOESY spectra (see Supporting Information).

Seventeen ϕ angle constraints were determined from the $^3J_{NH-C\alpha H}$ coupling constants, and they are shown in Figure 2. The $^3J_{NH-C\alpha H}$ coupling constants of four residues (Ala4, Val10, Cys16, and Cys24) were less than 5.5 Hz, and the ϕ angle restraints were determined in the range of $-90°$ to $-40°$. The $^3J_{NH-C\alpha H}$ coupling constants of 13 residues (Lys2, Cys8, Asp9, Phe11, Ser12, Leu13, Asp14, Thr17, Ile19, Cys20, Leu21, Val23, and Met25) were greater than 8.0 Hz, and the ϕ angle restraints were determined in the range of $-160°$ to $-80°$. Stereospecific assignments and χ^1 side chain torsion angle constraints were determined for three residues, Cys1, Cys8, and Cys20. The side chains of Cys1, Cys8, and Cys20 assume g^2g^3, g^2g^3, and g^2t^3 conformations, respectively. Therefore, these χ^1 angles were constrained in the range of 20° to 100° for Cys1 and Cys8, and 140° to 220° for Cys20.

Secondary Structure. Figure 2 represents the sequential NOE connectivities observed in the 200 ms NOESY spectrum at 288 K with $^3J_{NH-C\alpha H}$ coupling constants and slowly exchanging amide protons. Connectivities are categorized as strong, medium, weak, and very weak, according to the height of the bars. No NOE typically originating from an α-helical pattern was observed. On the contrary, some NOEs concerned with turn formations, i.e., between residues i and $i+2$, were obtained. Eleven backbone amide protons (Glu6, Cys8, Thr17, Ile19, Cys20, Leu21, Gly22, Val23, Cys24, Met25, and Trp26) were observed to exchange slowly, indicating the possibility that they may contribute to hydrogen bonds or belong to the peptide core region. These facts indicate that the major secondary structure features of ω-CTX TxVII are the β-sheet and several turns.

Structure Calculation and Evaluation. NMR experimental constraints for the structure calculation consisted of 432 distance and 20 dihedral angle constraints. The total of 432 distance constraints includes 106 intraresidue and 305 interresidue NOE distance constraints and an additional 21 constraints derived from hydrogen and disulfide bonds.

Simulated annealing calculations were started from 100 initial random structures, and we selected 20 final structures with the lowest energy. Structural statistics for the averaged and 20 converged structures were evaluated in terms of thier structural parameters (Table 1).

The RMS differences from the averaged coordinates were 0.50 ± 0.09 Å for the backbone atoms (N, C_α, C, and O) and 0.98 ± 0.13 Å for all heavy atoms. For the same atom selection, the mean pairwise RMS deviations of the 20 individual structures were 0.70 ± 0.22 and 1.42 ± 0.29 Å. Figure 3 shows the distribution of the number of distance

Table 1: Structural Statistics for ω-CTX TxVII[a]

structural parameter	20 converged structures	mean structure
RMSD from experimental distance constraints (Å)		
all (432)	0.039 ± 0.003	0.037
intraresidue (103)	0.054 ± 0.005	0.062
sequential (130)	0.027 ± 0.005	0.019
medium range ($2 \leq \|i-j\| \leq 4$) (62)	0.035 ± 0.006	0.031
long range ($\|i-j\| \geq 5$) (113)	0.036 ± 0.005	0.028
hydrogen bond and disulfide bond (21)	0.021 ± 0.017	0.015
RMSD from experimental dihedral constraints (deg) (20)	0.898 ± 0.247	0.588
energetic statistics (kcal mol^{-1})[b]		
F_{NOE}	37.47 ± 3.64	34.75
F_{tor}	1.00 ± 0.52	0.41
F_{repel}	21.18 ± 3.17	23.07
E_{L-J}	−29.87 ± 9.62	−33.19
RMSD from idealized geometry		
bonds (Å)	0.005 ± 0.0004	0.005
angles (deg)	0.739 ± 0.024	0.750
impropers (deg)	0.608 ± 0.053	0.639

[a] The 20 converged structures refer to the final set of dynamical simulated annealing structures starting from 100 initial random structures; the mean structure was obtained by restrained minimization of the averaged coordinates of the 20 individual structures. The number of each experimental constraint used in the calculations is given in parentheses. [b] F_{NOE}, F_{tor}, and F_{repel} are the energies related to the NOE violations, the torsion angle violations, and the van der Waals repulsion term, respectively. The values of the force constants used for these terms are the standard values, as depicted in the X-PLOR 3.1 manual. E_{L-J} is the Lennard-Jones van der Waals energy calculated with the CHARMm (*49*) empirical energy functions.

constraints. Most residues have more than 20 NOEs. All residues from Cys1 to Met25 indicate backbone RMSD values less than 0.50 Å (see Supporting Information). Only that of Trp26 at the C terminus is larger than 0.50 Å, but smaller than 1.00 Å. All residues indicate low RMSD values for all heavy atoms, except for Trp26. The angular order parameters of all of the residues are larger than 0.80, except for the value of Trp26. All of these values indicate that ω-CTX TxVII assumes a rigid conformation throughout the entire molecule.

Three-Dimensional Structure. Figure 4 shows a stereopair representation of the best-fit superposition of the backbone atoms (N, C_α, C, and O) for 20 converged structures. Disulfide bonds are shown in gray. The view in Figure 4B is a 90° rotation of that in Figure 4A around the vertical axis, which shows a β-sheet face. The three-dimensional structure of ω-CTX TxVII consists of a compact disulfide-bonded core and contains a β-sheet region composed of three short β-strands, i.e., β-strand 1 (Glu6 to Cys8), β-strand 2 (Ile19 to Leu21), and β-strand 3 (Gly22 to Met25) (Figure 5).

These three β-strands are linked by four turns involving residues Gln3 to Glu6 (turn 1), Asp9 to Phe11 (turn 2), Cys15 to Gly18 (turn 3), and Leu21 to Val23 (turn 4) (Figure 1). These turns are classified into a type II β-turn (turn 1), an inverse γ-turn (turn 2), a type I β-turn (turn3), and a nontypical one (turn 4).

DISCUSSION

Structure of ω-CTX TxVII. In the present study, we determined the three-dimensional structure of ω-CTX TxVII in an aqueous solution. The detailed structure of ω-CTX TxVII is described below.

The 20 final converged structures (Figure 4) were in good agreement with the NMR constraint data, in which the NOE distance and torsion angle violations were smaller than 0.5 Å and 5°, respectively. As a result, the deviations from idealized covalent geometry were very small, and the Lennard-Jones van der Waals energy was low (Table 1). These results indicate that the converged structures do not have distortions and nonbonded bad contacts.The entire backbone structure from Cys1 to Trp26 is well defined (Figure 3 and Supporting Information).

ω-CTX TxVII is composed of a triple-stranded antiparallel β-sheet comprising residues 6 to 8, 19 to 21, and 22 to 25 (Figure 5) and four turns. This can be classified as a β-sheet of topology +2x, −1 (*38*), as shown in Figure 6A. The three disulfide bonds in ω-CTX TxVII form the classical cystine knot motif (*39*−*42*) of toxic or inhibitory polypeptides. Two disulfide bonds, Cys1−Cys16 and Cys15−Cys24, constrain the peptide backbone for close spatial contact between the third β-turn and the N- and C-termini. The Cys8−Cys20 disulfide bond interconnects β-strands 1 and 2. As shown in Figure 5, the β-sheet involves a β-bulge (*38*), which is defined as a region between two consecutive β-type hydrogen bonds including two residues on one strand opposite a single residue on the other strand: the three residues are identified as positions 1, 2, and *x*. These residues of ω-CTX TxVII are (1, 2, *x*) = (Asp5, Glu6, Cys24) and their φ, ψ conformational angles are as follows: (ϕ_1, ψ_1) = (87°, 14°) and (ϕ_2, ψ_2) = (−107°, 148°) from the average of the final 20 structures. Generally, the position 1 residue values (φ, ψ) are approximately (ϕ_1, ψ_1) = (85°, 0°) and the position 2 residue values are approximately (ϕ_2, ψ_2) = (−90°, 150°) for the G1 type of β-bulge. Thus, the β-bulge of ω-CTX TxVII is classified as a G1 β-bulge, although Gly is located at position 1 in a typical G1 β-bulge. Turn 1, which is the type II tight turn, is associated with the G1 β-bulge in ω-CTX TxVII; position 1 of the G1 β-bulge is consistent with the position 3 of the type II turn.

Structural Comparison of ω-CTX TxVII with ω-CTX GVIA and MVIIA, N-type Calcium Channel Blockers. Figure 1 shows a comparison of the secondary structure elements and the disulfide bonds between ω-CTX TxVII, GVIA (*8*−*11*), and MVIIA (*13*). The distribution of the secondary structure elements of ω-CTX TxVII almost corresponds to those of ω-CTX GVIA and MVIIA. All of these conotoxins contain the G1 β-bulge with the associated type II tight turn, which is turn 1, consisting of residues 3 to 6. The residues identified in the G1 β-bulge in ω-CTX GVIA and MVIIA are (1, 2, *x*) = (Gly5, Ser6, Cys25) and (Gly5, Ala6, Cys24). The hydrogen bonds involved in the β-bulges in these three conotoxins contribute to the folding and the stability of the peptides to connect the N and C termini. The length of turn 4 of ω-CTX TxVII is different from those of ω-CTX GVIA and MVIIA because of insertions or deletions of the residues in the region linking β-strands 2 and 3.

As shown in Figure 6, the overall folding of ω-CTX TxVII (A) is similar to those of ω-CTX GVIA (B) and MVIIA (C). The β-sheet topology of ω-CTX TxVII is the same as that reported for ω-CTX GVIA and MVIIA, as shown in Figures 7B,C. In Figure 6, these three toxins form the same cystine knot motif. Despite their very low amino acid

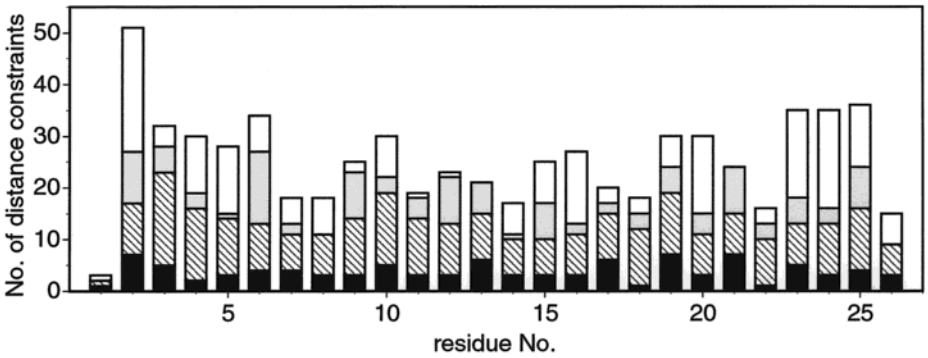

FIGURE 3: Distribution of the number of experimental distance constraints as a function of the sequence position of ω-CTX TxVII. Filled bars, intraresidue NOEs; hatched bars, sequential NOEs; speckled bars, medium-range NOEs; open bars, long-range NOEs. Each constraint is counted twice, once for each proton involved, except for intraresidue constraints, which are counted only once.

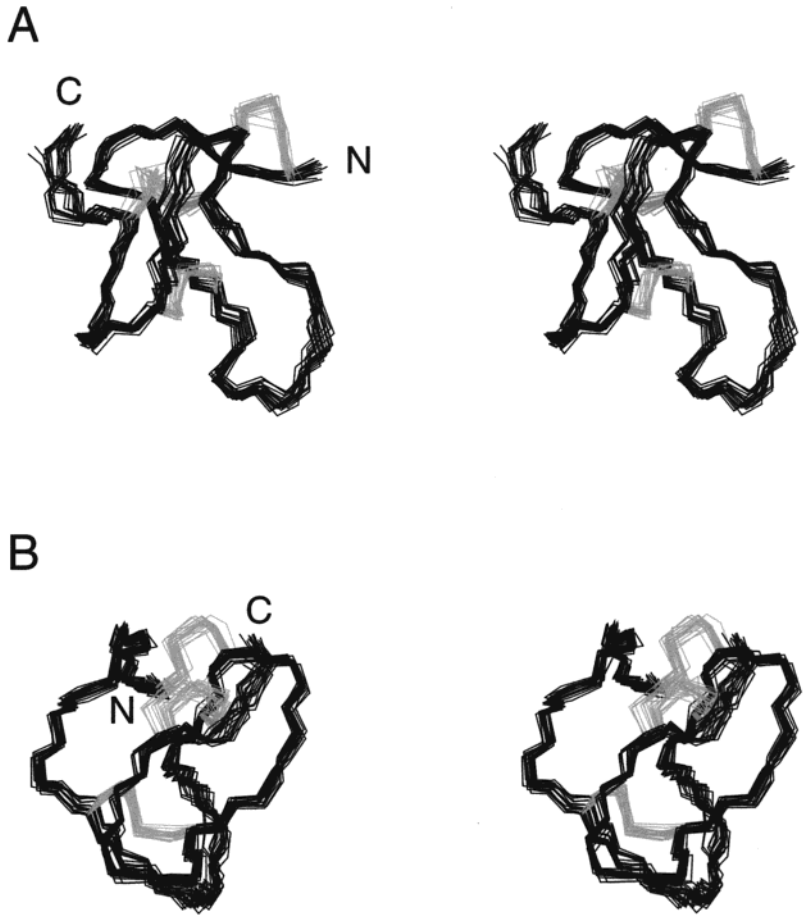

FIGURE 4: Stereoview of the superimposed backbone heavy atoms (N, C_α, and C) of the 20 converged structures of ω-CTX TxVII. Disulfide bonds are shown in gray. The view in Figure 4B is a 90° rotation of that in Figure 4A around the vertical axis. These figures were drawn by using MIDAS Plus (*50*).

sequence homology (Figure 1), these toxins share similar locations and orientations of the secondary structures in their three-dimensional structures. The only conserved sequence motif can be found in the spatial arrangement of the cystine residues in three dimensions. Thus, these disulfide bridges play a crucial role in the overall folding and stability of these peptides.

Figure 7 represents space-filling models of ω-CTX TxVII, GVIA, and MVIIA. Blue, red, and green indicate positively charged, negatively charged, and hydrophobic residues, respectively. The most critical residue, Tyr13, for the binding of ω-CTX GVIA and MVIIA to the N-type calcium channel is shown in yellow (*5, 43, 44*). Both ω-CTX GVIA and MVIIA have many basic amino acid residues. These positive charges are also important for the binding to the N-type calcium channel, and Lys2 is the most critical among them (*5*−*7*). It has been proposed that ω-CTX GVIA interacts with the vestibule of the N-type calcium channel via an electrostatic interaction with the positively charged residues (*45, 46*). However, the conserved Lys2 is the only positively charged residue in ω-CTX TxVII (Figure 1). There are several negative charges in the proximity of Lys2, resulting in cancellation of the positive charge. Furthermore, Tyr13 is replaced by a hydrophobic residue, Leu13, in ω-CTX TxVII. These may be the reasons why ω-CTX TxVII cannnot bind to the N-type calcium channel. Taken together, the

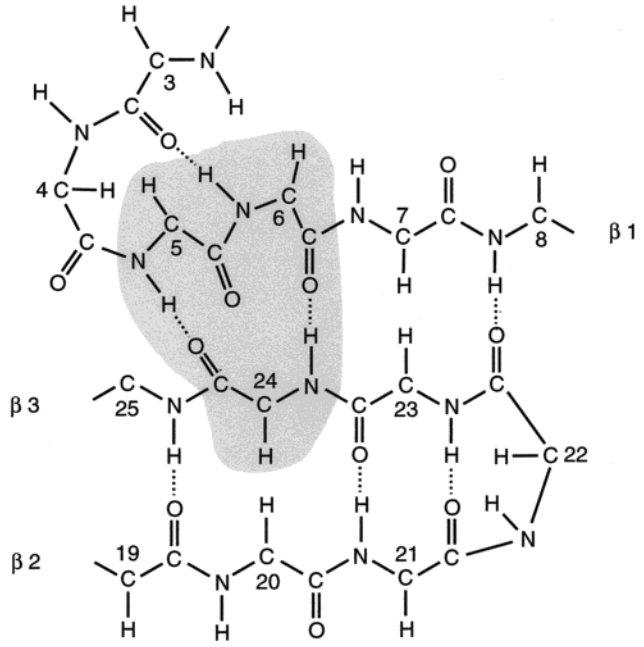

FIGURE 5: Schematic representation of the triple-stranded antiparallel β-sheet in ω-CTX TxVII. Hydrogen bonds are represented by broken lines. A β-bulge with the flanking type II tight turn (from Gln3 to Glu6) is also shown in gray.

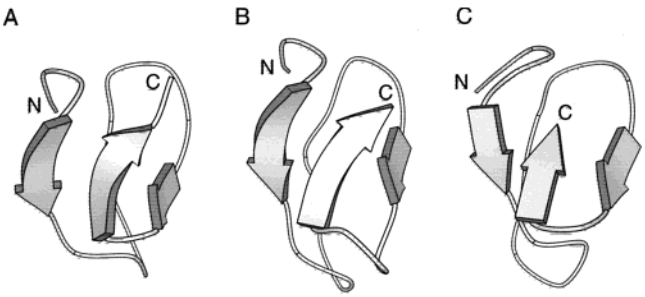

FIGURE 6: Schematic representations of the backbone polypeptide folding of (A) ω-CTX TxVII, (B) GVIA, and (C) MVIIA. The structural topology of the triple-stranded antiparallel β-sheet is shown. The coordinates of ω-CTX GVIA and MVIIA were obtained from the Protein Data Bank (PDB). The PDB accession codes are 1OMC and 1OMG, respectively. The figures were produced using MOLSCRIPT (*51*).

binding properties of ω-CTX TxVII may be quite different from those of ω-CTX GVIA and MVIIA, even though the overall folding of these three peptides is very similar.

The Structure−Activity Relationship of ω-CTX TxVII. ω-CTX TxVII is known to bind to mollusc L-type calcium channels (*19*). It has been reported that L-type calcium channels are blocked by three kinds of low molecular weight compounds, dihydropyridine (DHP), phenylalkylamine (PAA), and benzothiazepine (BTZ), and two kinds of peptides, calciseptine (*17*) and ω-agatoxin IIIA (*18*). The channel pore forming α_1 subunit has four homologous repeats, each with six α-helical transmembrane segments. The DHP binding sites of the L-type calcium channel are located on transmembrane segments 5 and 6 in domain III (IIIS5, IIIS6) and transmembrane segment 6 in domain IV (IVS6) of the α_1 subunit (*47*). It has been shown that two residues in IIIS5 (Thr1039 and Gln1043), seven residues in IIIS6 (Tyr1152, Ile1153, Ile1156, Phe1158, Phe1159, Met1160, and Met1161), and four residues in IVS6 (Tyr1463, Met1464, Ile1471, and Asn1472) contribute to DHP binding (numbering is according to rat brain α_{1C}). Nine of the 13 residues (Thr1039, Gln1043, Ile1153, Phe1158, Phe1159, Met1160, Tyr1463, Met1464, and Ile1471) are characteristic of the L-type α_1 subunit, and four residues (Tyr1152, Ile1156, Met1161, and Asn1472) are conserved in L-type and non-L-type α_1 subunits. The other two antagonist binding sites, for PAA and BTZ, are not the same as that for DHP, but they may be allosterically linked (*48*). The common characteristic of these three low molecular weight antagonists is that they all have aromatic rings.

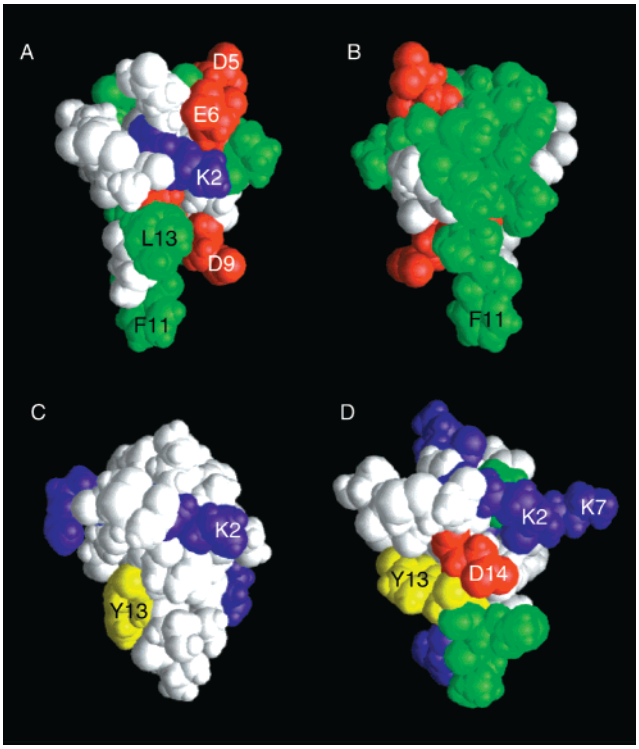

FIGURE 7: Space-filling models of (A, B) ω-CTX TxVII, (C) GVIA, and (D) MVIIA. Blue, red, and green indicate positively charged, negatively charged, and hydrophobic residues. One of the critical residues, Tyr13, in ω-CTX GVIA and MVIIA is shown in yellow. The view in Figure 7B is a 195° rotation of that in Figure 7A around the vertical axis.

On the other hand, ω-CTX TxVII is a much larger molecule as compared with these compounds. What is the common feature between this large molecule and the three smaller compounds? According to Figure 7, many hydrophobic residues are exposed on one side of the surface, which is the most remarkable characteristic of the spatial distribution of the residues in ω-CTX TxVII. In fact, such a hydrophobic residue distribution is unusual for other conotoxins and is not observed in either ω-CTX GVIA or MVIIA. The characteristics of the hydrophobic residues of ω-CTX TxVII correspond to the fact that all three compounds, DHP, PAA, and BTZ, have hydrophobic moieties (aromatic ring). In these three L-type calcium channel antagonists, these hydrophobic moieties may play an important role in the binding to the L-type calcium channel. Therefore, the exposed hydrophobic residues of ω-CTX TxVII may interact with the region such as the above-mentioned hydrophobic cluster of the α_1 subunit of the L-type calcium channel, which consists of 13 amino acid residues located in IIIS5, IIIS6, and IVS6. Interestingly, ω-CTX TxVII has only two residues with aromatic rings, Phe11 and Trp26, which is characteristic of the other three

L-type calcium channel antagonists. Thus, Phe11 and/or Trp26 may play a crucial role in the binding to the L-type calcium channel. These observations also suggest that ω-CTX TxVII may inhibit the mullusc L-type calcium current in the same manner as DHP, PAA, and BTZ. To address this in more detail, the binding properties of analogues in which Phe11 or Trp26 is replaced by another residue should be examined.

This solution structure of ω-CTX TxVII reported here should contribute to our understanding of the structure and the action of L-type calcium channel antagonists, and it will be useful in designing synthetic organic compounds to control specific types of calcium channels.

ACKNOWLEDGMENT

We thank Dr. Michael Fainzilber, of the Weizmann Institute, and Drs. Masami Takahashi, Jae-Il Kim, and Takao Matsuzaki, of the Mitsubishi Kasei Institute of Life Sciences, for helpful discussions.

SUPPORTING INFORMATION AVAILABLE

One table of NMR chemical shifts of ω-CTX TxVII ^{1}H resonances and one figure showing the backbone variability by residue. This material is available free of charge via the Internet at http://pubs.acs.org.

REFERENCES

1. Tsien, R. W., Ellinor, P. T., and Horne, W. A. (1991) *Trends Pharmacol. Sci. 12*, 349−354.
2. Miller, R. J. (1992) *J. Biol. Chem. 267*, 1403−1406.
3. Randall, A., and Tsien, R. W. (1995) *J. Neurosci. 15*, 2995−3012.
4. Olivera, B. M., Miljanich, G. P., Ramachandran, J., and Adams, M. E. (1994) *Annu. Rev. Biochem. 63*, 823−867.
5. Kim, J.-I., Takahashi, M., Ogura, A., Kohno, T., Kudo, Y., and Sato, K. (1994) *J. Biol. Chem. 269*, 23876−23878.
6. Kim, J.-I., Takahashi, M., Ohtake, A., Wakamiya, A., and Sato, K. (1995) *Biochem. Biophys. Res. Commun. 206*, 449−454.
7. Sato, K., Park, N.-G., Kohno, T., Maeda, T., Kim, J.-I., Kato, R., and Takahashi, M. (1993) *Biochem. Biophys. Res. Commun. 194*, 1292−1296.
8. Davis, J. H., Bradley, E. K., Miljanich, G. P., Nadasdi, L., Ramachandran, J., and Basus, V. J. (1993) *Biochemistry 32*, 7396−7405.
9. Pallaghy, P. K., Duggan, B. M., Pennington, M. W., and Norton, R. S. (1993) *J. Mol. Biol. 234*, 405−420.
10. Sevilla, P., Bruix, M., Santoro, J., Gago, F., Garcia, A. G., and Rico, M. (1993) *Biochem. Biophys. Res. Commun. 192*, 1238−1244.
11. Skalicky, J. J., Metzler, W. J., Ciesla, D. J., Galdes, A., and Pardi, A. (1993) *Protein Sci. 2*, 1591−1603.
12. Pallaghy, P. K., and Norton, R. S. (1999) *J. Pept. Res. 53*, 343−351.
13. Kohno, T., Kim, J.-I., Kobayashi, K., Kodera, Y., Maeda, T., and Sato, K. (1995) *Biochemistry 34*, 10256−10265.
14. Basus, V. J., Nadasdi, L., Ramachandran, J., and Miljanich, G. P. (1995) *FEBS Lett. 370*, 163−169.
15. Catterall, W. A., and Striessnig, J. (1992) *Trends Pharmacol. Sci. 13*, 256−262.
16. Hofmann, F., Biel, M., and Flockerzi, V. (1994) *Annu. Rev. Neurosci. 17*, 399−418.
17. de Weille, J. R., Schweitz, H., Maes, P., Tartar, A., and Lazdunski, M. (1991) *Proc. Natl. Acad. Sci. U.S.A. 88*, 2437−2440.
18. Mintz, I. M., Venema, V. J., Adams, M. E., and Bean, B. P. (1991) *Proc. Natl. Acad. Sci. U.S.A. 88*, 6628−6631.
19. Fainzilber, M., Lodder, J. C., van der Schors, R. C., Li, K. W., Yu, Z., Burlingame, A. L., Geraerts, W. P. M., and Kits, K. S. (1996) *Biochemistry 35*, 8748−8752.
20. Cruz, L. J. (1996) in *Natural Toxins II* (Singh, B. R., and Tu, A. T., Eds.) pp 155−167, Plenum Press, New York.
21. Sasaki, T., Feng, Z.-P., Scott, R., Grigoriev, N., Syed, N. I., Fainzilber, M., and Sato, K. (1999) *Biochemistry 38*, 12876−12884.
22. Mueller, L. (1987) *J. Magn. Reson. 72*, 191−196.
23. Rance, M., Sørensen, O. W., Bodenhausen, G., Wagner, G., Ernst, R. R., and Wüthrich, K. (1983) *Biochem. Biophys. Res. Commun. 117*, 479.
24. Jeener, J., Meier, B. H., Bachmann, P., and Ernst, R. R. (1979) *J. Chem. Phys. 71*, 4546−4553.
25. Macura, S., Huang, Y., Suter, D., and Ernst, R. R. (1981) *J. Magn. Reson. 43*, 259−281.
26. Bax, A., and Davis, D. G. (1985) *J. Magn. Reson. 65*, 355−359.
27. Pardi, A., Billerter, M., and Wüthrich, K. (1984) *J. Mol. Biol. 180*, 741−751.
28. Kline, A. D., Braun, W., and Wüthrich, K. (1988) *J. Mol. Biol. 204*, 675−724.
29. Hyberts, S. G., Marki, W., and Wagner, G. (1987) *Eur. J. Biochem. 164*, 625−635.
30. Wagner, G., Braun, W., Havel, T. F., Schaumann, T., Go, N., and Wüthrich, K. (1987) *J. Mol. Biol. 196*, 611−639.
31. Wüthrich, K., Billeter, M., and Braun, W. (1983) *J. Mol. Biol. 169*, 949−961.
32. Clore, G. M., Gronenborn, A. M., Nilges, M., and Ryan, C. A. (1987) *Biochemistry 26*, 8012−8023.
33. Nilges, M., Clore, G. M., and Gronenborn, A. M. (1988) *FEBS Lett. 229*, 317−324.
34. Brünger, A. T. (1992) *X-PLOR Manual, Version 3.1*, Yale University, New Haven, CT.
35. Ramachandran, G. N., Ramakrishnan, C., and Sasisekharan, V. (1963) *J. Mol. Biol. 7*, 95−99.
36. Hyberts, S. G., Goldberg, M. S., Havel, T. F., and Wagner, G. (1992) *Protein Sci. 1*, 736−751.
37. Wüthrich, K. (1986) *NMR of proteins and nucleic acids*, Wiley, New York.
38. Richardson, J. S. (1981) *Adv. Protein Chem. 34*, 167−339.
39. Pallaghy, P. K., Nielsen, K. J., Craik, D. J., and Norton, R. S. (1994) *Protein Sci. 3*, 1833−1839.
40. Narasimhan, L., Singh, J., Humblet, C., Guruprasad, K., and Blundell, T. (1994) *Nat. Struct. Biol. 1*, 850−852.
41. Issacs, N. W. (1995) *Curr. Opin. Struct. Biol. 5*, 391−395.
42. Norton, R. S., and Pallaghy, P. K. (1998) *Toxicon 36*, 1573−1583.
43. Lew, M. J., Flinn, J. P., Pallaghy, P. K., Murphy, R., Whorlow, S. L., Wright, C. E., Norton, R. S., and Angus, J. A. (1997) *J. Biol. Chem. 272*, 12014−12023.
44. Nadasdi, L., Yamashiro, D., Chung, D., Tarczy-Hornoch, K., Adriaenssens, P., and Ramachandran, J. (1995) *Biochemistry 34*, 8076−8081.
45. Ellinor, P. T., Zhang, J. F., Horne, W. A., and Tsien, R. W. (1994) *Nature 372*, 272−275.
46. Flinn, J. P., Pallaghy, P. K., Lew, M. J., Murphy, R., Angus, J. A., and Norton, R. S. (1999) *Eur. J. Biochem. 262*, 447−455.
47. Striessnig, J., Grabner, M., Mitterdorfer, J., Hering, S., Sinnegger, M. J., and Glossmann, H. (1998) *Trends Pharmacol. Sci. 19*, 108−115.
48. Glossmann, H., and Striessnig, J. (1990) *Rev. Physiol. Biochem. Pharmacol. 114*, 1−105.
49. Brooks, B. R., Bruccoleri, R. E., Olafson, B. D., States, D. J., Swaminathan, S., and Karplus, M. (1983) *J. Comput. Chem. 4*, 187−217.
50. Ferrin, T. E., Huang, C. C., Jarvis, L. E., and Langridge, R. (1988) *J. Mol. Graphics 6*, 13−27.
51. Kraulis, P. (1991) *J. Appl. Crystallogr. 24*, 946−950.

BI001506X